Protonation of Histidine and Histidine−Tryptophan Interaction in the Activation of the M2 Ion Channel from Influenza A Virus†

Atsushi Okada, Takashi Miura, and Hideo Takeuchi*

Graduate School of Pharmaceutical Sciences, Tohoku University, Aobayama, Sendai 980-8578, Japan

Received December 15, 2000; Revised Manuscript Received March 7, 2001

ABSTRACT: The M2 protein of influenza A virus forms a homotetramer ion channel in the lipid membrane. The channel is specific for proton conductance and is activated by low pH with a transition midpoint at pH 5.7. We have studied the structure of the transmembrane domain of the M2 ion channel by using UV resonance Raman spectroscopy, with special attention to the side chains of histidine (His37) and tryptophan (Trp41) residues. The Raman spectra provide direct evidence that the imidazole ring of His37 is protonated upon channel activation at low pH. Concomitantly, the UV resonance Raman scattering from Trp41 shows an unusual intensity change, which is ascribed to a cation−π interaction between the protonated (cationic) imidazole ring of His37 and the indole ring of Trp41. The protonation of His37 and the Raman intensity change of Trp41 do not occur in the presence of amantadine that blocks the M2 ion channel. These observations clearly show that the protonation of His37 and concomitant cation−π interaction with Trp41 is a key step in the activation of the M2 ion channel. The His37−Trp41 interaction associated with the channel activation is explained by assuming a conformational transition of His37 induced by electrostatic repulsion among the protonated imidazole rings of four His37 residues in the tetramer channel. Trp41 may play a role in stabilizing the channel open state through cation−π interaction with His37. A molecular model for the activation of M2 ion channel is proposed on the basis of the gating mechanism.

The M2 protein, an integral membrane protein of influenza A virus, forms a proton-specific transmembrane ion channel, which is activated at acidic pH (*1*, *2*). The importance of the M2 ion channel in the life cycle of influenza A virus is proved by the finding that the virus infection is dose-dependently inhibited by amantadine (1-aminoadamantane, AMT[1]), which blocks the M2 ion channel (*3*−*5*). The M2 ion channel is considered to play roles in both early and late stages of virus infection (*6*). Once the virus is internalized into a host cell by receptor-mediated endocytosis, it is delivered to a secondary endosome, which has a mildly acidic internal pH (*7*). The virion-associated M2 ion channel activated in the acidic endosomal compartment permits protons to enter into the virion interior. The decrease of pH within the virion induces dissociation of coat proteins such as hemagglutinin and matrix protein M1 (*8*, *9*), an essential step for subsequent entry of the virus genome into the nucleus of the host cell. In a late stage of the infection, many copies of the M2 protein expressed in the host cell form ion channels in the trans Golgi network to neutralize the pH of acidic vesicular compartments by releasing protons. The pH regulation in the Golgi vesicular compartments is necessary for protection of acid-sensitive hemagglutinin from denaturing during the transport of the glycoprotein to the host cell surface prior to virus assembly (*10*).

The polypeptide chain of the M2 protein is composed of 97 amino acid residues with a putative 19-residue single transmembrane domain (residues 25−43) located between the N- and C-terminal hydrophilic regions (*11*). The transmembrane domain is rich in hydrophobic residues with the exceptions of Ser31, His37, and Trp41. An analysis of ion channel activity for mixtures of wild-type M2 protein and its AMT-resistant mutants has shown that the minimal active unit of the M2 ion channel is a homotetramer (*12*), which is stabilized by noncovalent interactions in the transmembrane domain and by disulfide linkages in the N-terminal ectomembrane region (*13*−*15*). Mutations in the transmembrane domain cause significant changes in channel activity and AMT sensitivity, suggesting that the transmembrane domain forms a pore for ion transport (*1*, *16*, *17*). Duff and Ashley have demonstrated that a 25-residue peptide (NH_2-Ser-Ser-Asp-Pro[25]-Leu-Val-Val-Ala-Ala-Ser[31]-Ile-Ile-Gly-Ile-Leu-His[37]-Leu-Ile-Leu-Trp[41]-Ile-Leu[43]-Asp-Arg-Leu-COOH, M2-TMP) encompassing the transmembrane domain (underlined) actually forms AMT-sensitive proton channels in lipid bilayers (*18*).

The structure of the M2-TMP ion channel has been investigated by spectroscopic methods. Duff et al. examined the circular dichroism (CD) of M2-TMP incorporated into phosphatidylcholine liposomes to find that the peptide main chain of M2-TMP was predominantly α-helical in the absence and presence of AMT (*19*). Cross and co-workers

† This work was supported in part by a Grant-in-Aid (No. 11440169) from the Ministry of Education, Science, Sports, and Culture of Japan.

* Corresponding author. Phone/Fax: +81-22-217-6855. E-mail: takeuchi@mail.cc.tohoku.ac.jp.

[1] Abbreviations: AMT, amantadine; CD, circular dichroism; ImD^+, N-deuterated imidazolium; IE18C6, *N*,*N*′-bis(2-(3-indolyl)ethyl)-4,13-diaza-18-crown-6; M2-TMP, a 25-residue peptide encompassing the putative transmembrane domain of M2 protein; POPE, 1-palmitoyl-2-oleoyl-L-α-phosphatidylethanolamine; POPS, 1-palmitoyl-2-oleoyl-L-α-phosphatidylserine; SDS, sodium dodecyl sulfate; UVRR, ultraviolet resonance Raman.

10.1021/bi0028441 CCC: $20.00
Published on Web 04/27/2001

studied the tilt angle of the M2-TMP helix with respect to the lipid membrane by solid-state NMR (*20*−*22*). From NMR spectra of oriented samples of peptides whose amide nitrogens were labeled with ^{15}N, the helix tilt angle was found to be in a range of 32−38° irrespective of the membrane thickness and AMT binding. Kukol et al. measured infrared dichroism spectra of M2-TMP containing a ^{13}C-labeled carbonyl group at Ala29 or Ala30 to obtain a helix tilt angle of 32° and a rotational pitch angle of −60° for Ala29 (*23*). These spectroscopic studies have provided important information on the main-chain structure of the M2-TMP ion channel. On the other hand, no experimental data are available for the structures of individual side chains.

Among the amino acid residues of the M2 protein, the side chain of His37 is believed to play an important role in activation of the M2 ion channel. The proton conductance of the wild-type M2 ion channel shows a 50-fold increase on going from pH 8.2 to pH 4.5 with a transition midpoint at pH 5.77 (*4*). On the other hand, the mutation of His37 to Ala, Gly, or Glu makes the proton conductance insensitive to pH (*1*, *4*). This finding suggests that the activity of M2 ion channel is regulated by protonation of the imidazole side chain of His37, the only amino acid residue protonatable around pH 6. However, no experimental evidence has been reported for the direct link between the protonation of His37 and the channel activation. Trp41, which is located one helix pitch apart from His37, is also considered to play an important role in channel activity because the replacement of Trp41 with Ala results in a loss of proton flux through the channel (*16*).

In this study, we have investigated the side-chain structures of His37 and Trp41 in M2-TMP ion channels incorporated into phospholipid bilayer membranes by using ultraviolet resonance Raman (UVRR) spectroscopy. UVRR spectroscopy is a powerful tool for structural investigations of aromatic residues in membrane-bound proteins (*24*). Analysis of UVRR spectra has shown that the imidazole ring of His37 is actually protonated at acid pH, where the M2 ion channel is activated. Concomitant with the protonation of His37, Trp41 shows an unusual change of Raman intensity, which can be ascribed to an interaction between the indole ring of Trp41 and a cation, presumably the protonated imidazole ring of His37. A model for the activation of M2 ion channel is proposed on the basis of the His37 protonation and His37−Trp41 interaction.

EXPERIMENTAL PROCEDURES

Materials. M2-TMP was synthesized on an Applied Biosystems Model 431A automated peptide synthesizer from amino acid derivatives protected by the 9-fluorenylmethoxycarbonyl group. The peptide was cleaved from the resin and then purified by HPLC on gel-filtration and reversed-phase columns. 1-Palmitoyl-2-oleoyl-L-α-phosphatidylethanolamine (POPE) and 1-palmitoyl-2-oleoyl-L-α-phosphatidylserine (POPS) were purchased from Avanti Polar Lipids and used as received. *N*,*N*′-Bis(2-(3-indolyl)ethyl)-4,13-diaza-18-crown-6 (IE18C6) was synthesized and purified by the literature method (*25*, *26*). The final product was identified by elemental analysis and mass spectrometry.

Sample Preparation. M2-TMP channels were reconstituted into phospholipid membranes as follows. Typically, 15 mg (5.6 μmol) of M2-TMP was codissolved with 4 equiv each of POPE and POPS in 6 mL of chloroform/methanol (1:1 v/v). The solution was spread as a thin layer onto the wall of a round-bottom flask by drying under vacuum. Excess drying time (>24 h) was taken to ensure complete removal of the solvent. Water (7 mL) was then added to the flask, and the lipid was hydrated under vortexing. In preparing the samples for UVRR measurements, 8 mM KNO_3 was added to the hydration water as an internal standard of Raman intensity. The opaque suspension was sonicated in a bath sonicator until the suspension became clear. The hydration and sonication were performed at 35 °C, about 10 °C above the gel to liquid-crystalline transition temperature (∼25 °C) of the lipid vesicles (*27*). In pH titration experiments, an aliquot of liposome suspension was mixed with the same volume of K_2HPO_4 (20 mM)/citric acid (10 mM) buffer at varied pH. The pH of the suspension was measured before and after the spectral measurement to ensure no pH shift. The K^+ concentration in the buffer was adjusted to a constant value of 40 mM by adding KCl. The final concentration of M2-TMP in the liposome suspension was 300 μM. For the samples of CD and 229 nm UVRR measurements, the final concentration of M2-TMP was reduced to 100 and 150 μM, respectively, by scaling down the amounts of peptide, lipid, and other reagents used in the preparation of liposomes. When preparing D_2O suspensions of liposomes, methanol-OD and D_2O were used instead of methanol and H_2O in the procedures described above.

A 1:1 complex of IE18C6 with K^+ was prepared by mixing KCl (0.5 mM) with IE18C6 (0.2 or 0.4 mM) in methanol. $LiNO_3$ (5 mM) was also added to the solution as an internal standard of Raman intensity. The ionic radius of Li^+ is too small to fit with the hole of 18-crown-6, and the addition of $LiNO_3$ did not affect the absorption and UVRR spectra.

Acquisition and Analysis of Spectral Data. Circular dichroism (CD) spectra were recorded on a Jasco J-720 polarimeter at 5 °C using a 1 mm quartz cell thermostated with a constant temperature circulating bath. Absorption spectra were recorded on a Hitachi U-3300 spectrophotometer. UVRR spectra were excited with 229 or 244 nm continuous wave radiation from an intracavity frequency-doubled Ar ion laser (Coherent Innova 300 FReD) and recorded on a UV Raman spectrometer (Jasco TR-600UV) equipped with a CCD detector (Princeton Instruments LN/CCD-1752). The suspension of M2-TMP-incorporated liposomes was recirculated by using a peristaltic pump through a capillary cell (inner diameter, 2 mm) and a reservoir immersed in an ice bath. The temperature of the sample was about 5 °C. For the K^+ complex of IE18C6, a quartz spinning cell was used.

UVRR spectra recorded at varied pH (pD) were analyzed by using the Hill equation (*28*, *29*):

$$M + hH^+ \rightleftharpoons M{\cdot}hH^+ \quad (1)$$

$$Y_{pH} = [H^+]^h/(K + [H^+]^h) \quad (2)$$

where M stands for M2-TMP, h for the Hill coefficient, K for the dissociation constant, and Y_{pH} for the fraction of protonated protein at that pH. Since the intensity of a Raman band of protonated protein (I_{pH}) is proportional to Y_{pH}, the

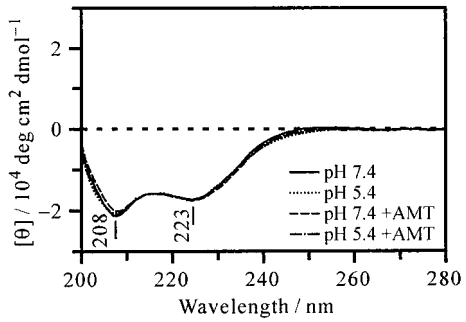

FIGURE 1: Circular dichroism spectra of M2-TMP incorporated into POPE/POPS liposomes at pH 7.4 and 5.4 in the absence and presence (1 mM) of AMT. The concentrations of M2-TMP, POPE, and POPS are 100, 400, and 400 μM, respectively.

ratio of I_{pH} to the intensity at a reference pH (I_{pHr}) is expressed as

$$\frac{I_{pH}}{I_{pHr}} = \frac{(10^{pHr})^h + 10^{pK}}{(10^{pH})^h + 10^{pK}} \quad (3)$$

In this study, pH (pD) 5.4 was chosen for the reference pH as done in a previous Hill equation analysis of the M2 ion channel activity (*4*). Values of *K* and *h* were obtained from experimentally observed $I_{pH}/I_{5.4}$ by the nonlinear least-squares method using a commercially available software package (MathCad).

RESULTS

Secondary Structure Monitored by Circular Dichroism. Figure 1 shows the CD spectra of M2-TMP incorporated into POPE/POPS liposomes. The lipid composition employed here is identical to that used in the channel activity assay of M2-TMP (*18*). The CD spectrum at pH 7.4 (solid line) exhibits two negative peaks at 208 and 223 nm characteristic of α-helical structure (*30*). Substantially the same spectrum is observed at pH 5.4 and in the presence of AMT (dotted, dashed, and dash-dotted lines). These observations indicate that neither the activation at acidic pH nor the inhibition by AMT significantly affects the secondary structure of M2-TMP.

Protonation of His37 Monitored by UVRR Spectroscopy. It is usually difficult to detect His Raman bands in UVRR spectra of peptides and proteins containing both His and Trp residues. This is because strong UVRR scattering from Trp covers weak Raman signals from His. To overcome the difficulty, we have recorded Raman spectra of M2-TMP in D_2O with 244 nm excitation for the following two reasons. First, when the imidazole ring of His is protonated (deuterated) in acidic D_2O medium, the N-deuterated imidazolium (ImD^+) gives a characteristic Raman band around 1410 cm^{-1}, which is much stronger than the Raman bands of neutral His and serves as a measure of the protonation (deuteration) of His (*31*, *32*). Second, the UV absorption of the Trp indole ring shows a minimum around 240 nm, and the resonance enhancement of Trp Raman scattering can be reduced when excited at 244 nm, thus giving minimal interference to His Raman bands (*33*, *34*).

Traces A and B of Figure 2 show 244 nm excited Raman spectra of M2-TMP-incorporated liposomes suspended in D_2O buffers at pD 7.4 and 5.4, respectively. The 1048 cm^{-1} band is due to NO_3^- added as an internal intensity standard. Even with 244 nm excitation, Raman scattering from Trp dominates the spectra. The Raman bands assignable to indole ring vibrations of Trp41 are labeled with W followed by their mode numbers (*35*). The 1456 cm^{-1} band contains a contribution from the imide C═O stretch of the Asp23−Pro24 linkage (*36*). Although no His Raman bands are identified in the spectrum at pD 7.4, the spectrum at pD 5.4 exhibits a weak band at 1407 cm^{-1} assignable to ImD^+ of His37 (Figure 2B). Spectral changes associated with the pD change are more clearly seen in the difference spectrum, B − A (Figure 2C). In the difference spectrum, the ImD^+ 1407 cm^{-1} band of His37 shows up as a positive peak. The assignment of the 1407 cm^{-1} band to ImD^+ is supported by the observation that the difference spectrum of amino acid L-His between pD 4 and pD 8 consists of a dominant positive peak at 1410 cm^{-1} (Figure 2D). No other amino acids give a UV resonance Raman band around 1410 cm^{-1} that shows up only in acidic D_2O solution (*35*).

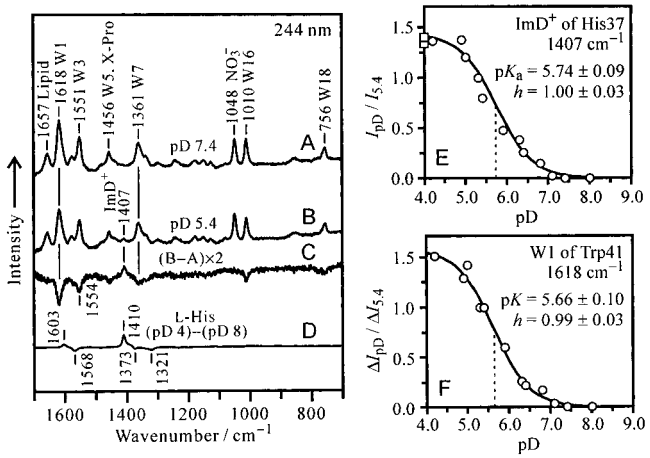

FIGURE 2: Left panel: UV (244 nm) resonance Raman spectra of M2-TMP incorporated into POPE/POPS liposomes at pD 7.4 (A) and 5.4 (B). Trace C shows the difference (B − A), the intensity of which is amplified by a factor of 2. Raman bands of Trp41 are labeled with W followed by their mode numbers (*35*). X-Pro stands for the imide II mode of the X-Pro linkage. The 1657 cm^{-1} band is ascribed to the C═C stretch of the lipids. The 1048 cm^{-1} band is due to NO_3^- added as an internal intensity standard. The 1407 cm^{-1} band in traces B and C is assigned to N-deuterated imidazolium of His37. The concentrations of M2-TMP, POPE, and POPS are 300, 1200, and 1200 μM, respectively. The bottom spectrum shows the difference between pD 4 and pD 8 for amino acid L-His (10 mM). Right panel: Raman intensity plotted as a function of pD for the 1407 (E, ImD^+) and 1618 cm^{-1} (F, W1) bands of M2-TMP incorporated into POPE/POPS liposomes. The intensity of the 1407 cm^{-1} band at each pD (I_{pD}) is normalized to that at pD 5.4 ($I_{5.4}$). On the other hand, the intensity difference between a pD value and pD 8.0 (ΔI_{pD}) is normalized to that at pD 5.4 ($\Delta I_{5.4}$) for the 1618 cm^{-1} band. In each plot, the curve shows a fit with eq 3, and the dashed line indicates the midpoint of transition. The squares in (E) indicate the intensity of the 1407 cm^{-1} band in the presence of SDS, which is expected to destroy the liposome.

To determine the pK_a value of His37, we have examined UVRR spectra in a pD range of 4.0−8.0. The measured Raman intensity of the 1407 cm^{-1} ImD^+ band relative to that at the reference pD 5.4 ($I_{pD}/I_{5.4}$) is plotted against pD in Figure 2E (open circles). Analysis of the data with eq 3 gives $pK_a = 5.74 \pm 0.09$ and $h = 1.00 \pm 0.03$ (solid curve in Figure 2E). The pK_a value of His37 obtained here is identical to the p*K* value (5.77 ± 0.06) of M2 channel activation

reported previously (*4*). Furthermore, our value of *h* is equal, within experimental error, to the value (0.96 ± 0.14) obtained from the activation assay (*4*). Since two independent equilibria in a protein are unlikely to give identical p*K* and *h* values, the coincidence of both parameters gives evidence for a close link between the protonation of His37 and the activation of the M2 ion channel.

The M2 ion channel is a homotetramer and contains four His37 residues. To determine how many His37 residues are protonated in the active channel state, we have mixed a suspension of M2-TMP-incorporated liposome with 50 mM sodium dodecyl sulfate (SDS), which is expected to destroy the liposome and to make the M2-TMP peptide exposed to the solvent. The Raman intensity of the 1407 cm^{-1} ImD^+ band after the addition of SDS at pD 4.0 is plotted in Figure 2E as squares. As seen in the figure, the addition of SDS does not increase the Raman intensity of the ImD^+ band, indicating that all four His37 residues of the tetramer are already protonated (deuterated) in the membrane-bound active state of the M2-TMP channel.

UVRR Intensity and Structure of Trp41. In addition to the protonation of His37, the pD change from 7.4 to 5.4 causes intensity decreases of Trp41 Raman bands as evidenced by negative peaks in the difference spectrum (Figure 2C). We have examined the pD dependence of the intensity of the W1 (1618 cm^{-1}) band, the strongest Raman band of Trp41 in 244 nm excited spectra. The effect of pD change on the W1 intensity may be represented by the change of intensity measured from that at pD 8.0 (ΔI_{pD}). The ΔI_{pD} value relative to that at the reference pD 5.4 ($\Delta I_{5.4}$) is plotted as a function of pD in Figure 2F. By applying eq 3 to this plot, we obtain pK = 5.66 ± 0.10 and h = 0.99 ± 0.03, which correspond well with the pK_a and h values obtained for the protonation of His37 (Figure 2E). This observation clearly shows that the Raman intensity change of Trp41 occurs in conjunction with the protonation of His37.

To further investigate the structural origin of the Raman intensity change of Trp41, we have recorded UVRR spectra with 229 nm excitation, which produces strong Raman scattering from Trp. Traces A and B of Figure 3 show the 229 nm excited Raman spectra of M2-TMP-incorporated liposomes suspended in H_2O buffers at pH 7.4 and 5.4, respectively. Peak wavenumbers of Trp Raman bands are slightly shifted to higher wavenumbers from those in the spectra of Figure 2 because the proton attached to the indole nitrogen is not replaced by deuterium in the spectra of Figure 3. As seen in the difference spectrum (Figure 3C), the pH change from 7.4 to 5.4 causes an intensity *increase* of Trp41 Raman scattering, which is in sharp contrast to the intensity *decrease* observed with 244 nm excitation. The intensity increase of the W16 (1010 cm^{-1}) band is plotted against pH in Figure 3D in the same way as done for the Raman intensity of the W1 band excited at 244 nm (Figure 2F). This plot gives the values of pK = 5.52 ± 0.21 and h = 1.01 ± 0.06, which are identical to those obtained from the Raman intensity decrease observed in the 244 nm excited spectra. Thus, the Raman intensity *increase* observed with 229 nm excitation and the intensity *decrease* observed with 244 nm excitation must arise from the same structural origin.

It is known that UVRR intensity of Trp is sensitive to the strength of hydrogen bonding at the indole nitrogen and to the environmental hydrophobicity of the indole ring (*37*).

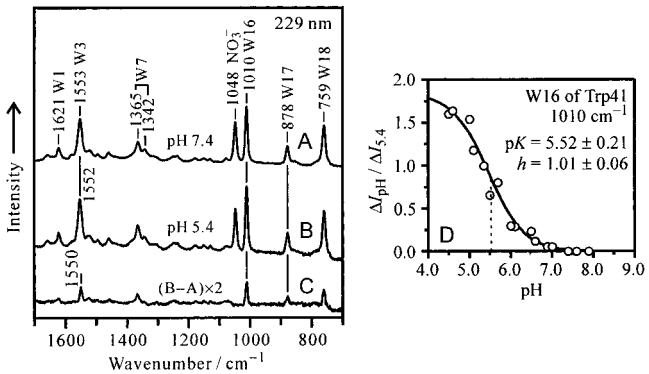

FIGURE 3: Left panel: UV (229 nm) resonance Raman spectra of M2-TMP incorporated into POPE/POPS liposomes at pH 7.4 (A) and 5.4 (B). Trace C shows the difference (B − A), the intensity of which is amplified by a factor of 2. Raman bands of Trp41 are labeled with W followed by their mode numbers (*35*). The 1048 cm^{-1} band is due to NO_3^- added as an internal intensity standard. The concentrations of M2-TMP, POPE, and POPS are 150, 600, and 600 μM, respectively. Right panel: (D) pH dependence of the 1010 cm^{-1} (W16) Raman intensity of M2-TMP incorporated into POPE/POPS liposomes. The intensity difference between a pD value and pH 8.0 (ΔI_{pH}) is normalized to that at pH 5.4 ($\Delta I_{5.4}$). The curve shows a fit with eq 3, and the dashed line indicates the midpoint of transition.

An increase in hydrogen-bonding strength or in hydrophobicity causes a red shift of the B_b electronic absorption band around 220 nm with a concomitant increase in intensity. The change of B_b absorption results in an increase of Raman scattering excited at a wavelength longer than 220 nm. Accordingly, the Raman intensity behavior does not differ largely between 229 and 244 nm excitation if a change occurs in hydrogen bonding and/or in environmental hydrophobicity (*37*). Actually, however, the 229 and 244 nm excited Raman intensities of Trp41 change in opposite directions upon activation of the M2-TMP channel. It is unlikely that a simple change in hydrogen bonding or in environmental hydrophobicity is the origin of the Raman intensity change of Trp41. Detailed analysis of the 229 nm excited Raman spectra in Figure 3 also denies this possibility as described below.

The wavenumber of the W17 band is a marker of hydrogen bonding at the indole nitrogen, and the observed W17 wavenumber (878 cm^{-1}, Figure 3A) indicates a hydrogen bond of medium strength such as with a water molecule (*38*). Since the W17 wavenumber does not change with pH (Figure 3B), the hydrogen-bonding state at the indole NH site must remain unchanged upon activation of the channel. Thus, the state of hydrogen bonding is irrelevant to the Raman intensity change of Trp41. The relative intensity of the W7 doublet at 1365/1342 cm^{-1} reflects the environmental hydrophobicity of the indole ring, and an increase in hydrophobicity increases the intensity ratio I_{1365}/I_{1342} (*39*). For M2-TMP, the doublet intensity ratio is high at both pH 7.4 and pH 5.4 (Figure 3A,B), indicating that Trp41 is located in a hydrophobic environment, which remains unchanged upon channel activation. Thus, the environmental hydrophobicity is not responsible for the Raman intensity change of Trp41. The wavenumber of the W3 band is a marker of the absolute value of the $\chi^{2,1}$ torsional angle ($|\chi^{2,1}|$) about the $C_\alpha-C_\beta-C_3-C_2$ linkage (*40*). Using the relationship between the W3 wavenumber and $|\chi^{2,1}|$ (*41*), the $|\chi^{2,1}|$ value of Trp41 is calculated to be about 100° from the observed W3 wavenumber (1553

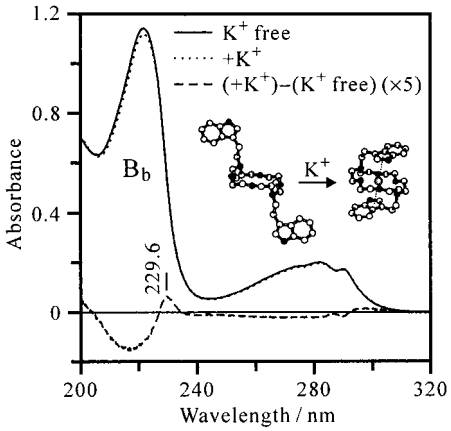

FIGURE 4: UV absorption spectra of IE18C6 in the absence and presence (500 μM) of K^+. The crown ether was dissolved in methanol at a concentration of 200 μM. The dashed line shows the effect of K^+ binding amplified by a factor of 5.

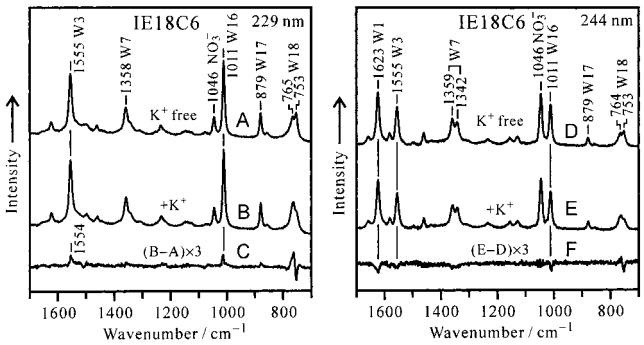

FIGURE 5: UV resonance Raman spectra of IE18C6 in the absence (A and D) and presence (B and E) of K^+. The spectra in the left panel (A−C) are excited at 229 nm and those (D, E) in the right panel at 244 nm. The difference spectra (C and F) are amplified by a factor of 3. The concentrations of IE18C6 and KCl are 400 and 500 μM, respectively.

cm^{-1}) at pH 7.4 (Figure 3A). Since the W3 band appears at 1550 cm^{-1} (a 3 cm^{-1} downshift) in the difference spectrum between pH 5.4 and pH 7.4 (Figure 3C), the $|\chi^{2,1}|$ value is likely to become a few degrees smaller in the active channel state. However, such a small change in $|\chi^{2,1}|$ is improbable to directly affect the Raman intensity.

Since the Raman intensity change of Trp41 occurs in conjunction with the protonation of His37 as described above, a possible origin of the Raman intensity change is an interaction between His37 and Trp41, i.e., between the protonated (cationic) imidazole ring of His37 and the π electrons of the Trp41 indole ring. To study the effects of cation$-\pi$ interactions on the electronic states of the indole ring, we have examined UV absorption and UVRR spectra of IE18C6. IE18C6 has two indole side arms attached to the nitrogens of the diaza-18-crown-6 ring, and the two indole rings sandwich a K^+ ion trapped in the hole of 18-crown-6 (*25*, *26*). Figure 4 compares UV absorption spectra of IE18C6 in the absence and presence of K^+. The difference spectrum (dashed line) reveals a small red shift and a weakening of the B_b absorption at ~220 nm upon complexation with K^+. Changes in the intensity of the 229 and 244 nm excited Raman spectra of IE18C6 (Figure 5) are more sensitive in reflecting complexation with K^+ than are the minor variations in the absorption spectra. The binding of K^+ to IE18C6 causes an intensity increase (left panel, 229 nm) and a decrease (right panel, 244 nm) of the indole Raman scattering. The general trend in intensity change parallels that observed for M2-TMP upon activation of the channel at acidic pH (pD) (Figures 2 and 3). Accordingly, the most plausible origin of the Raman intensity change of Trp41 is a cation$-\pi$ interaction between the protonated imidazole ring of His37 and the indole ring of Trp41. It is also noted that the cation$-\pi$ interaction is not so strong as to cause significant wavenumber shifts of the indole ring vibrations.

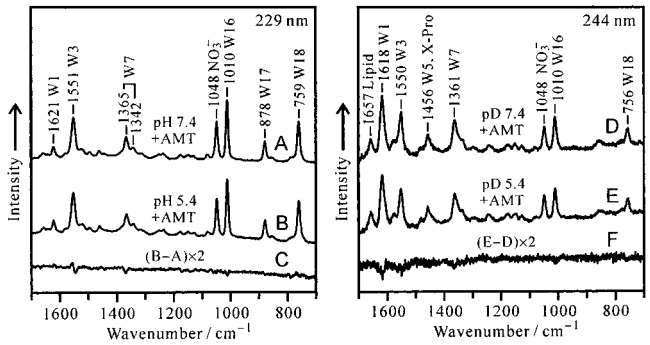

FIGURE 6: UV resonance Raman spectra of M2-TMP incorporated into POPE/POPS liposomes at pH (pD) 7.4 (A and D) and 5.4 (B and E) in the presence of 2 mM AMT. The spectra in the left panel (A−C) are excited at 229 nm and those (D, E) in the right panel at 244 nm. The difference spectra (C and F) are amplified by a factor of 2. The concentrations of M2-TMP, POPE, and POPS, respectively, are 150, 600, and 600 μM for 229 nm excitation and 300, 1200, and 1200 μM for 244 nm excitation.

Effect of AMT Binding on the Structures of His37 and Trp41. We have also recorded the 229 and 244 nm excited Raman spectra of the M2-TMP channel in the presence of AMT, a blocker of the M2 ion channel (Figure 6). As shown in the difference spectrum between pH (pD) 7.4 and 5.4 (Figure 6C,F), the spectral changes upon acidification in the presence of AMT are much smaller than those in the absence of AMT (Figures 2C and 3C). This observation indicates that the binding of AMT almost completely inhibits both the protonation of His37 and the consequent cation$-\pi$ interaction between His37 and Trp41. The inhibition of M2 channel activity by AMT is thus closely related to the inhibition of His37 protonation. Further comparison of the spectra in the presence of AMT (Figure 6) with those recorded under the corresponding pH (pD) and excitation wavelength conditions but in the absence of AMT (Figures 2 and 3) reveals that the binding of AMT causes a 2 cm^{-1} downshift (from 1553 to 1551 cm^{-1}) of the W3 band of Trp41 and an increase of Trp41 Raman scattering at both excitation wavelengths of 229 and 244 nm. The downshift of the W3 band, a conformation marker, indicates a few degrees decrease of $|\chi^{2,1}|$ (*41*). The UVRR intensity increase common to the 229 and 244 nm excited spectra suggests a small red shift of the B_b absorption, which may be caused by an increase in the strength of hydrogen bonding and/or in the environmental hydrophobicity of Trp41 (*37*). Since the wavenumber of W17 (878 cm^{-1}), a hydrogen bond marker, does not change with the binding of AMT (compare Figures 3A and 6A), the red shift of the B_b absorption is ascribed to an increase in the environmental hydrophobicity of Trp41. It is concluded that the binding of AMT to the M2-TMP channel induces a structural change that involves a small increase in hydrophobic interaction and a decrease

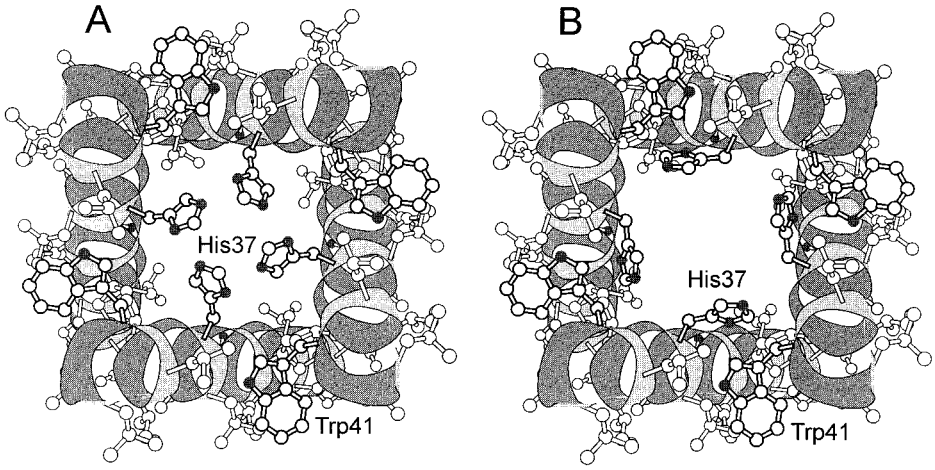

FIGURE 7: Models for the closed (A) and open (B) forms of the transmembrane domain of the M2 ion channel viewed from the C-terminal side. The side chains of His37 and Trp41 are drawn with thick lines. The shaded circles indicate nitrogen atoms.

in $|\chi^{2,1}|$ of Trp41 together with a prohibitive decrease of proton accessibility to the imidazole ring of His37.

DISCUSSION

In this study, we have examined the structure of the M2-TMP channel by UVRR spectroscopy with special attention to His37 and Trp41. Analysis of the UVRR spectra has provided direct evidence that the channel activation is closely linked with the protonation of four His37 residues in the tertramer channel. Another important finding is that a cation$-\pi$ interaction occurs between the protonated imidazole ring (imidazolium) of His37 and the indole ring of Trp41 in the active channel state. These structural changes are inhibited by AMT. The results of this study provide some clues to understanding the activation mechanism of the M2 ion channel.

Proton Conductance Mechanism. Since the mutation of His37 to Ala, Gly, or Glu diminishes the pH sensitivity of M2 channel activity, His37 is considered to play a key role in the proton-transfer process (*1, 4*). Two types of mechanisms, shuttle and gating, have been proposed for the role of His37 in M2 channel activity. In the initial step of the shuttle mechanism (*17, 42*), a proton coming from one side of the channel binds to one of two nitrogens of the neutral imidazole ring of His37 and the imidazole ring becomes imidazolium. Next, the proton already attached to the other imidazole nitrogen is released toward the other side of the channel. After the net proton translocation mediated by the His37 shuttle, the imidazole ring returns to the initial state through tautomerism. The tautomerism of the imidazole ring is fully utilized in the shuttle mechanism. In the gating mechanism (*43*), on the other hand, the proton conductance is regulated by a conformational change of the channel. At neutral to alkaline pH, the imidazole rings of all four His37 residues are directed toward the center of the channel and occlude the channel pore ("closed" form). At acidic pH, every imidazole ring acquires an additional proton, and electrostatic repulsion among the positively charged imidazole rings causes a movement of the rings away from each other, leaving the channel pore open for a chain of water molecules that relays protons ("open" form). An important difference between the two mechanisms resides in the number of protonated His37 residues. In the shuttle mechanism, protonation of His37 occurs transiently and only one or two His37 residues in the tetramer channel are protonated at any one time (*17, 42*). In contrast, all His37 residues are protonated during the channel open state in the gating mechanism (*43*). The present UVRR finding that all His37 residues are protonated in the active channel state lends support to the gating mechanism.

Role of His37−Trp41 Interaction. In addition to the imidazole ring of His37, the indole ring of Trp41 is also important in maintaining the proper channel activity of M2. Substitution of alanine for Trp41 greatly reduces the proton conductance and pH sensitivity (*16*). The cation$-\pi$ interaction between His37 and Trp41 detected by UVRR spectroscopy may be related to the functional importance of Trp41. To examine the structural implications of the cation$-\pi$ interaction, we have built a model for the transmembrane domain of the M2 ion channel. In the model building, a 19-residue (Pro25−Leu43) helix was first constructed by using standard structural parameters for α-helix (*44, 45*). The helix was then tilted by 32° and rotated about the helix axis so that the amide I vibrational transition moment of Ala29 makes an angle of −60° with respect to the helix tilt plane (*23*). The other subunits in the tetramer were generated by 4-fold rotational symmetry operation in a left-handed supercoil structure (*17*). The interchain center-to-center distance was assumed to be 11.5 Å (10.5 Å at the closest approach; *17*). The conformations of His37 and Trp41 were taken from a library for preferred rotamers of these residues in an α-helix (*46*). To avoid steric clash with the main-chain helix, the His side chain prefers the T+ ($\chi^1 = -178°$, $\chi^2 = 82°$), G′− ($\chi^1 = -67°$, $\chi^2 = 87°$), G′+ ($\chi^1 = -81°$, $\chi^2 = 95°$), and T− ($\chi^1 = -170°$, $\chi^2 = -121°$) rotamers. On the other hand, three rotamers are favored by Trp: T+ ($\chi^1 = 178°$, $\chi^{2,1} = 81°$), T− ($\chi^1 = -179°$, $\chi^{2,1} = -108°$), and G′+ ($\chi^1 = -70°$, $\chi^{2,1} = 117°$). Since the W3 wavenumber observed in UVRR spectra has indicated that the $|\chi^{2,1}|$ value is close to 100°, the $\chi^{2,1}$ angles in the Trp41 rotamers may be replaced by ±100°.

In the closed form of the gating mechanism, the imidazole rings of four His37 residues should be directed toward the center of the channel pore. This arrangement is achieved if His37 takes the T+ or T− rotamer. Here we adopt the T+ rotamer because this rotamer can be stabilized by hydrogen

bonds between adjacent imidazole rings. Of the three possible rotamers of Trp41, the G′+ rotamer is improbable because the indole ring clashes with the imidazole ring of His37 on the same helix. In the T− rotamer, on the other hand, the indole ring becomes too close to an adjacent helix. The remaining rotamer T+ is the most probable rotamer for Trp41. Figure 7A shows our model for the closed form viewed from the C-terminal side. The His37 side chains occlude the channel pore, and the Trp41 side chains seem to play a role in stabilizing the tetramer through hydrophobic interactions with Leu and Ile side chains of an adjacent helix. The indole ring of Trp41 is located far away from the imidazole ring of His37, suggesting no interactions between the two rings in the closed form.

According to the gating mechanism, the His37 imidazole rings move away from the channel pore on going from the closed to open form. This structural change can be achieved simply by rotating the His37 side chain about the $C_\alpha-C_\beta$ bond, corresponding to a rotamer change from T+ to G+ (Figure 7B). As a result, the imidazole ring of His37 moves closer (<5 Å) to the indole ring of Trp41 on an adjacent helix. Since the His37 imidazole ring is protonated (cationic) in the open form, the close proximity of the two rings may account for the cation−π interaction detected by UVRR spectroscopy. A possible role of the cation−π interaction between His37 and Trp41 is to stabilize the open form by partially neutralizing the positive charge on the imidazole ring of His37 with negative charges of π electrons on the indole ring of Trp41. It is known that Trp is the best suited amino acid for cation−π interactions (*47*). This may be one of the reasons why Trp41 is strictly conserved among naturally occurring mutants of the M2 protein (*16*).

Mechanism of Inhibition by AMT. The UVRR spectra have shown that protonation of His37 does not take place in the presence of AMT, an inhibitor of the M2 ion channel. This observation provides evidence that AMT inhibits M2 channel activity by preventing His37 from being protonated even at acidic pH. Since the protonation of His37 is a trigger of proton conduction in both shuttle and gating mechanisms, AMT blocks the initial step of proton conduction. A neutron diffraction study has revealed that the AMT binding site is located about 6 Å from the center of the membrane bilayer (*48*). The location of AMT binding corresponds to the areas of Val27−Ser 31 and His37−Trp41 in the M2 ion channel. Actually, point mutations in the Val27−Ser31 region make M2 protein resistant to AMT (*16*). On the other hand, effects of mutations in the His37−Trp41 region on the AMT sensitivity are not clarified because such mutations drastically change the channel activity (*4*, *16*). Possibly, the hydrophobic adamantane ring of AMT bound to the Val27−Ser31 and His37−Trp41 regions blocks water permeation to His37, thus preventing the protonation of His37 even at acidic pH. As described in the Results section, the environmental hydrophobicity of Trp41 increases in the presence of AMT. This observation is consistent with the AMT binding to the His37−Trp41 region. Changes in helix assembly of the M2 ion channel upon AMT binding might also contribute to the increase of environmental hydrophobicity of Trp41.

In conclusion, we have presented experimental evidence for the protonation of His37 upon activation of the M2 ion channel by using UVRR spectroscopy. In the active channel state, the protonated imidazole ring of His37 is shown to interact with the indole ring of Trp41 through cation−π interaction. AMT, an antiviral drug, blocks the M2 ion channel by preventing the protonation of His37. These UVRR findings are the first structural information about the side chains of amino acid residues composing the M2 ion channel. The present study demonstrates the utility of UVRR spectroscopy in detecting His protonation and His−Trp cation−π interactions in membrane-bound proteins.

REFERENCES

1. Pinto, L. H., Holsinger, L. J., and Lamb, R. A. (1992) *Cell 69*, 517−528.
2. Chizhmakov, I. V., Geraghty, F. M., Ogden, D. C., Hayhurst, A., Antoniou, M., and Hay, A. J. (1996) *J. Physiol. 494*, 329−336.
3. Shimbo, K., Brassard, D. L., Lamb, R. A., and Pinto, L. H. (1996) *Biophys. J. 70*, 1335−1346.
4. Wang, C., Lamb, R. A., and Pinto, L. H. (1995) *Biophys. J. 69*, 1363−1371.
5. Davies, W. L., Grunert, R. R., Haff, R. F., McGahen, J. W., Neumayer, E. M., Paulshock, M., Watts, J. C., Wood, T. R., Hermann, E. C., and Hoffmann, C. E. (1964) *Science 144*, 862−863.
6. Ciampor, F., Cmarko, D., Cmarkova, J., and Zavodska, E. (1995) *Acta Virol. 39*, 171−181.
7. White, J. M., Hoffman, L. R., Arevalo, J. H., and Wilson, I. A. (1997) in *Structural Biology of Viruses* (Chiu, W., Burnett, R. M., and Garcea, R. L., Eds.) pp 80−104, Oxford University Press, Cambridge.
8. Martin, K., and Helenius, A. (1991) *Cell 67*, 117−130.
9. Bron, R., Kendal, A. P., Klenk, H. D., and Wilschut, J. (1993) *Virology 195*, 808−811.
10. Takeuchi, K., and Lamb, R. A. (1994) *J. Virol. 68*, 911−919.
11. Lamb, R. A., Zebedee, S. L., and Richardson, C. D. (1985) *Cell 40*, 627−633.
12. Sakaguchi, T., Tu, Q., Pinto, L. H., and Lamb, R. A. (1997) *Proc. Natl. Acad. Sci. U.S.A. 94*, 5000−5005.
13. Sugrue, R. J., and Hay, A. J. (1991) *Virology 180*, 617−624.
14. Holsinger, L. J., and Lamb, R. A. (1991) *Virology 183*, 32−43.
15. Castrucci, M. R., Hughes, M., Calzoletti, L., Donatelli, I., Wells, K., Takada, A., and Kawaoka, Y. (1997) *Virology 238*, 128−134.
16. Holsinger, L. J., Nichani, D., Pinto, L. H., and Lamb, R. A. (1994) *J. Virol. 68*, 1551−1563.
17. Pinto, L. H., Dieckmann, G. R., Gandhi, C. S., Papworth, C. G., Bramann, J., Shaughnessy, M. A., Lear, J. D., Lamb, R. A., and DeGrado, W. F. (1997) *Proc. Natl. Acad. Sci. U.S.A. 94*, 11301−11306.
18. Duff, K. C., and Ashley, R. H. (1992) *Virology 190*, 485−489.
19. Duff, K. C., Kelly, S. M., Price, N. C., and Bradshaw, J. P. (1992) *FEBS Lett. 311*, 256−258.
20. Kovacs, F. A., and Cross, T. A. (1997) *Biophys. J. 73*, 2511−2517.
21. Kovacs, F. A., Denny, J. K., Song, Z., Quine, J. R., and Cross, T. A. (2000) *J. Mol. Biol. 295*, 117−125.
22. Song, Z., Kovacs, F. A., Wang, J., Denny, J. K., Sheker, S. C., Quine, J. R., and Cross, T. A. (2000) *Biophys. J. 79*, 767−775.
23. Kukol, A., Adams, P. D., Rice, L. M., Brunger, A. T., and Arkin, I. T. (1999) *J. Mol. Biol. 286*, 951−962.
24. Hashimoto, S., Obata, K., Takeuchi, H., Needleman, R., and Lanyi, J. K. (1997) *Biochemistry 36*, 11583−11590.
25. De Wall, S. L., Meadows, E. S., Barbour, L. J., and Gokel, G. W. (1999) *J. Am. Chem. Soc. 121*, 5613−5614.
26. De Wall, S. L., Meadows, E. S., Barbour, L. J., and Gokel, G. W. (2000) *Proc. Natl. Acad. Sci. U.S.A. 97*, 6271−6276.
27. Epand, R. M., and Lim, W. (1995) *Biosci. Rep. 15*, 151−160.
28. Hill, A. V. (1910) *J. Physiol. (London) 40*, 4−7.
29. Fersht, A. (1977) *Enzyme Structure and Mechanism*, Freeman, New York.

30. Johnson, W. C., Jr. (1988) *Annu. Rev. Biophys. Biophys. Chem. 17*, 145−166.
31. Tasumi, M., Harada, I., Takamatsu, T., and Takahashi, S. (1982) *J. Raman Spectrosc. 12*, 149−151.
32. Hashimoto, S., and Takeuchi, H. (1998) *J. Am. Chem. Soc. 120*, 11012−11013.
33. Su, C., Wang, Y., and Spiro, T. G. (1990) *J. Raman Spectrosc. 21*, 435−440.
34. Sweeney, J. A., and Asher, S. A. (1990) *J. Phys. Chem. 94*, 4784−4791.
35. Harada, I., and Takeuchi, H. (1986) in *Spectroscopy of Biological Systems* (Clark, R. J. H., and Hester, R. E., Eds.) pp 113−175, John Wiley and Sons, New York.
36. Takeuchi, H., and Harada, I. (1990) *J. Raman Spectrosc. 21*, 509−515.
37. Matsuno, M., and Takeuchi, H. (1998) *Bull. Chem. Soc. Jpn. 71*, 851−857.
38. Miura, T., Takeuchi, H., and Harada, I. (1988) *Biochemistry 27*, 88−94.
39. Harada, I., Miura, T., and Takeuchi, H. (1986) *Spectrochim. Acta, Part A 42*, 307−312.
40. Miura, T., Takeuchi, H., and Harada, I. (1989) *J. Raman Spectrosc. 20*, 667−671.
41. Maruyama, T., and Takeuchi, H. (1997) *Biochemistry 36*, 10993−11001.
42. Schwighofer, K. J., and Pohorille, A. (2000) *Biophys. J. 78*, 150−163.
43. Sansom, M. S. P., Kerr, I. D., Smith, G. R., and Son, H. S. (1997) *Virology 233*, 163−173.
44. Barlow, D. J., and Thornton, J. M. (1988) *J. Mol. Biol. 201*, 601−619.
45. Momany, F. A., McGuire, R. F., Burgess, A. W., and Scheraga, H. A. (1975) *J. Phys. Chem. 79*, 2361−2381.
46. McGregor, M. J., Islam, S. A., and Sternberg, M. J. E. (1987) *J. Mol. Biol. 198*, 295−310.
47. Mecozzi, S., West, A. P., Jr., and Dougherty, D. A. (1996) *Proc. Natl. Acad. Sci. U.S.A. 93*, 10566−10571.
48. Duff, K. C., Gilchrist, P. J., Saxena, A. M., and Bradshaw, J. P. (1994) *Virology 202*, 287−293.

BI0028441